Chaos, Solitons and Fractals 166 (2023) 112915

Contents lists available at ScienceDirect

Chaos, Solitons and Fractals

journal homepage: www.elsevier.com/locate/chaos

About ghost transients in spatial continuous media

Àngel Calsina [a,b], Sílvia Cuadrado [a,*], Blai Vidiella [b,c], Josep Sardanyés [b,*]

[a] Departament de Matemàtiques, Universitat Autònoma de Barcelona, Cerdanyola del Vallès, 08193, Barcelona, Spain
[b] Centre de Recerca Matemàtica, Edifici C, Cerdanyola del Vallès, 08193, Barcelona, Spain
[c] Evolution of Networks Lab, Institute of Evolutionary Biology (UPF-CSIC), Passeig Marítim de la Barceloneta 37, 08003, Barcelona, Spain

ARTICLE INFO

MSC:
35B32
92B99
92D40

Keywords:
Ghosts
Reaction–diffusion dynamics
Saddle–node bifurcations
Scaling laws
Spatial ecology
Tipping points
Transients

ABSTRACT

The impact of space on ecosystem dynamics has been a matter of debate since the dawn of theoretical ecology. Several studies have revealed that space usually involves an increase in transients' times, promoting the so-called supertransients. However, the effect of space and diffusion in transients close to bifurcations has not been thoroughly investigated. In non-spatial deterministic models such as those given by ordinary differential equations transients become extremely long in the vicinity of bifurcations. Specifically, for the saddle–node (s–n) bifurcation the time delay, τ, follows $\tau \sim |\mu - \mu_c|^{-1/2}$; μ and μ_c being the bifurcation parameter and the bifurcation value, respectively. Such long transients are labeled delayed transitions and are governed by the so-called ghosts. Here, we explore a simple model with intra-specific cooperation (autocatalysis) and habitat loss undergoing a s–n bifurcation using a partial differential equations (PDE) approach. We focus on the effects of diffusion in the ghost extinction transients right after the tipping point found at a critical habitat loss threshold. Our results show that the bifurcation value does not depend on diffusion. Despite transients' length typically increase close to the bifurcation, we have observed that at extreme values of diffusion, both small and large, extinction times remain long and close to the well-mixed results. However, ghosts lose influence at intermediate diffusion rates, leading to a dramatic reduction of transients' length. These results, which strongly depend on the initial size of the population, are shown to remain robust for different initial spatial distributions of cooperators. A simple two-patch metapopulation model gathering the main results obtained from the PDEs approach is also introduced and discussed. Finally, we provide analytical results of the passage times and the scaling for the model under study transformed into a normal form. Our findings are discussed within the framework of ecological transients.

1. Introduction

The importance of transients in ecological systems has been highlighted by a multitude of authors due to the relevant timescales in ecological dynamics [1–5] and their importance in applications, for instance in adaptive management of renewable resources [2] or sustainment of ecosystems after tipping points [6,7]. Transient phenomena have been described in marine and terrestrial ecosystems and in experimental research [4]. Here, mathematical concepts such as bifurcations i.e. tipping points [8], saddles [1], and the role of processes operating on different timescales [9], among others (see below) play a crucial role in transients' behaviors.

Ecological systems typically have different timescales, and such dynamics on multiple scales make transients likely to appear [9–11]. For instance, if the fast-timescale dynamics are on an ecologically-relevant scale and the slow-time scale is fast enough, then transients will be ecologically relevant [2]. A clear example of this is found in spruce-budworm dynamics [12], where insect dynamics occur on a very short timescale with population changes within a few years. However, the population of forest trees changes significantly over a period of decades. This interaction can be considered as a constant number of trees and consider the insect dynamics, to finally consider that the population dynamics of trees respond to the average population density of insects rather than to the annual insect density.

Saddles have been suggested as another mechanism causing transients. Saddles are unstable equilibria with some stable directions and the orbits slow down while approaching a saddle, causing long transients. A multitude of ecological dynamical models has revealed the presence of saddles, including simple models for two-species prey–predator [9], competition [13], or quantitative genetics [2,14]. In fact, some transient dynamical outcomes in experimental studies with the flour beetle suggested the pass through a saddle towards a period-two fixed point [1]. Several food chain models have also shown long,

* Corresponding authors.
E-mail addresses: silvia@mat.uab.cat (S. Cuadrado), jsardanyes@crm.cat (J. Sardanyés).

https://doi.org/10.1016/j.chaos.2022.112915
Received 19 August 2022; Received in revised form 29 October 2022; Accepted 14 November 2022
Available online 8 December 2022

complex transients due to another class of saddle-like sets: the chaotic saddles. These involve orbits entering into this (fractal) set that behaves chaotically for a finite amount of time, giving place to a chaotic transient towards another stable state [15–19]. Other transient-generator mechanisms have been suggested for ecological systems, including coupled oscillators, stochasticity, saddle–node ghosts (firstly proposed in [20]), and spatial systems (see [4] for a review). Regarding spatial models, integro-difference equations with alternating reproduction and dispersal have revealed long transients [21], also illustrating that spatial and temporal scales may be intimately connected [2]. Spatial models based on coupled map lattices [21–23] and on metapopulations [5] have revealed both the presence of very long transients.

Bifurcations are responsible for qualitative changes in dynamics as parameters are varied [24,25], and they are currently a hot topic of research in Ecology within the context of so-called tipping points, critical transitions, transients, and early warning signals [26–31]. For the saddle–node (s–n) bifurcation, clearly identified in laboratory experiments for electronic circuits [32], solid-state lasers [33], and yeast cell cultures [34], extremely long transients arise just after the bifurcation. These transients are labeled as delayed transitions or ghosts [25,35]. In short, the s–n bifurcation involves the collision and consequent annihilation of equilibrium points. This annihilation actually involves the jump of these two equilibria to the complex phase space [36–38], and, despite they are not found in the real numbers phase space, they still continue influencing the flows therein. This is why the orbits' delays right after this bifurcation are said to be governed by a ghost [6,7,20,25,36,37,39]. Transients close to bifurcations follow well-defined scaling laws relating the length of these transients with how far the bifurcation parameter is to its bifurcation value [25,40]. Such scaling properties are found both in continuous-time (flows) and discrete-time (maps) dynamical systems. For instance, the length of transients, τ, for the s–n scale as $\tau \sim |\mu - \mu_c|^{-1/2}$ for flows and maps [25,36,37], where μ and μ_c are the bifurcation parameter and bifurcation value, respectively. Remarkably, this scaling law has been identified experimentally in an electronic circuit [32].

S–n bifurcations typically arise in dynamical systems with strong nonlinearities such as positive feedbacks due to facilitation [7,8,20] or intra-specific cooperation (i.e., autocatalysis) [20,36,38,39,41,42]. Specifically, facilitation processes occurring in plants in dryland is hypothesized to be the key-mechanism leading to their tipping points, making them abrupt and not smooth [43–46]. Typically, cooperation provides a fitness benefit [47] which often depends on the size of the population i.e., Allee effect [48]. Intra-specific cooperation [49] is found in a multitude of species including food sharing in social insects [49,50], vampire bats [49], and primates [51], in the reproduction of marine species such as urchins, sponges, or cnidarians [52], where fertilization between individuals largely depends on population density. Other autocatalytic processes can be found in the growth and reproduction of yeast cells [34], in cancer cell populations via autocrine signaling [53], and in recovery dynamics after mass extinctions [54]. Other mathematical models have revealed s–n bifurcations in apoptotic switches in *Drosophila* [55], host-endosymbionts dynamics in arthropods [56], or gene regulatory networks [20], to cite a few.

Despite the extensive research on transients in ecological dynamical systems, there are still some unanswered questions. As previously mentioned, several modeling approaches point to the direction that space typically makes transients longer [57], but, is this the case for near-to-bifurcation transient phenomena? What are the properties of ghost transients in spatially-extended systems? How does diffusion affect transients' scaling laws compared to the predictions by well-mixed models? How does the initial spatial distribution of cooperators impact ghosts? Despite previous numerical attempts using metapopulation [20] and cellular automata [58] models have identified spatial ghosts, how spatial correlations and diffusion shape transients' lengths and scaling laws right after a s–n bifurcation remain poorly explored. In this article, we investigate these questions by studying a dynamical system of autocatalytic cooperators under habitat loss. Previous research indicated that this system, in the well-mixed setting, suffers a s–n bifurcation towards a monostable, extinction state [38,59]. Here, we have built a one-dimensional spatial model of this system using partial differential equations (PDEs). We focus on the effect of diffusion in the extinction transients and their scaling properties close to the s–n bifurcation and on the role of the initial distribution of cooperators in such transients. The most remarkable results of the PDE approach are shown to be explained by a simple two-patch metapopulation model. We also introduce a normal form for the spatial s–n bifurcation and analytically calculate transients' properties.

2. Reaction–diffusion model

In this section, we introduce the model we use to investigate the transients and their scaling properties right after a saddle–node (s–n) bifurcation considering spatial correlations. To do so, we use a reaction–diffusion system which is a generalization, taking space into account, of a mean-field model considering cooperation in growth (ecological facilitation or autocatalysis) and intra-specific competition. The mean-field model (the reaction function) reads:

$$\frac{du}{dt} = ku^2(1-\theta-u) - \epsilon u = f(u), \tag{1}$$

where u denotes the population numbers of a self-cooperative species. Note that the intrinsic growth term here is ku^2 (with $k > 0$), which involves hyperbolic growth (faster than growth of the form ku, typically considered in populations with exponential reproduction). This nonlinear growth has been widely used to model autocatalytic and cross-catalytic dynamics in species with intra-specific cooperation [8,38,59] and in hypercycles [58,60], respectively. The growth of the population is constrained by a logistic function with carrying capacity equal one and including the fraction of habitat destroyed $\theta \in [0,1]$. Note that when $\theta = 1$ no available space is found and the population cannot grow. The population is assumed to decay exponentially proportionally to $\epsilon > 0$. The dynamics of Eq. (1) has been widely studied in Refs. [8,38,59]. Roughly, this system has three equilibrium points given by $p_0 = 0$, and the pair

$$p_\pm = \frac{1}{2}\left(1-\theta \pm \sqrt{(1-\theta)^2 - 4r}\right),$$

with $r = \epsilon/k$. Before the bifurcation, p_0 is locally asymptotically stable while he equilibrium points p_+ and p_- are a stable node and a saddle point. These interior equilibria collide at the bifurcation value $\theta_c = 1-2\sqrt{r}$ in a s–n bifurcation. Right after the bifurcation, extremely long transients (governed by so-called ghosts) for large enough population values are found towards the single remaining equilibrium, the origin, which is globally asymptotically stable [59] (see Fig. 1b). These long transients, labeled as delayed transitions [25,35], are known to follow the inverse square-root scaling law in the deterministic limit, which involves a power law decay of the transient times as the bifurcation parameter is tuned above the bifurcation value (see the upper panels in Fig. 1b). The same model, transformed into a map, has been recently analyzed using holomorphic dynamics i.e., dynamics in the complex plane, to investigate the properties of the node and the saddle having jumped at the complex phase space after the bifurcation. This study revealed that these two equilibria become unstable spirals in the complex plane [38].

The model above is here studied considering a one-dimensional continuous space (Fig. 1a). We denote by $u(x,t)$ the density of individuals at spatial position x at time t and we assume that the dynamics of the population are given by the following reaction–diffusion equation (partial differential equation, PDE) in one spatial dimension

$$u_t = Du_{xx} + f(u), \quad x \in (0,1) \tag{2}$$

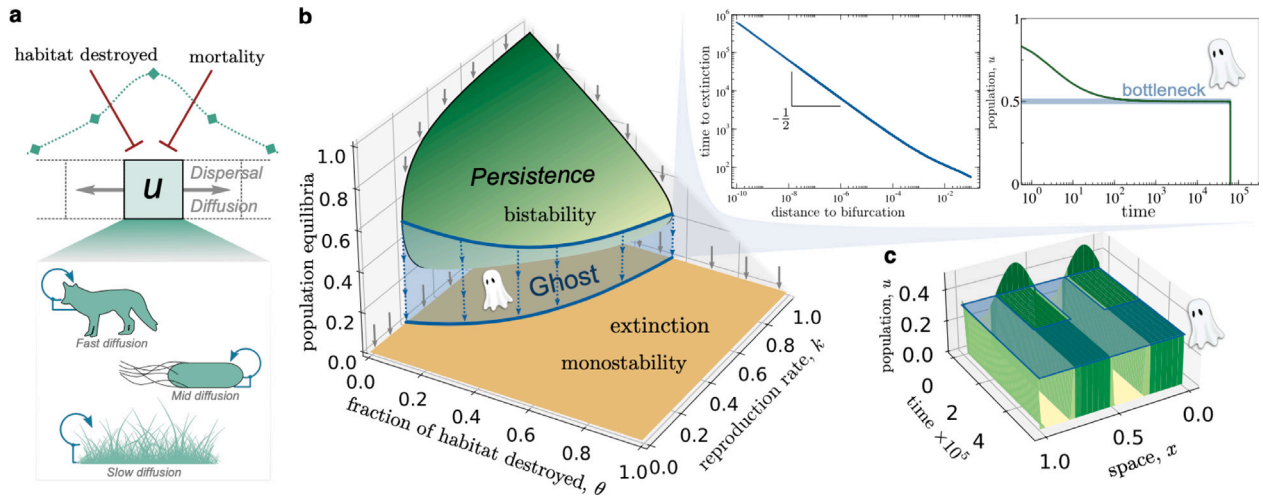

Fig. 1. (a) Schematic diagram of the system studied, which considers cooperators interacting in a one-dimensional spatial domain under habitat destruction. (b) Phase diagram showing the saddle–node bifurcation curve (blue line) in the parameter space (k, θ) with $\epsilon = 0.05$ for $du/dt = f(u)$, Eq. (1). The area below the green surface denotes the parameter region of bistability, where $u_\pm \in \mathbb{R}^+$, and the system can either persist or become extinct depending on $u(0)$. At the bifurcation curve the node and the saddle collide, and beyond this curve $u_\pm \in \mathbb{C}$, u_0 being a global attractor. Right after this bifurcation, the extinction times experience bottlenecks causing delays that follow an inverse square-root scaling law with respect to the bifurcation distance (small upper plots, computed numerically with a fourth-order Runge–Kutta method with time stepsize 0.1). (c) Characteristic extinction dynamics considering Eq. (2) with $D = 0$, here with $\epsilon = 0.1$. (For interpretation of the references to color in this figure legend, the reader is referred to the web version of this article.)

with diffusion coefficient or dispersal rate $D > 0$ and Neumann boundary conditions assuming that the individuals do not leave when they reach the boundary,

$$u_x(0,t) = u_x(1,t) = 0 \tag{3}$$

and where the reaction term is given by Eq. (1).

3. Results

3.1. PDE model: Analytical results

First, we study the steady states of the initial boundary value problem

$$\begin{cases} u_t = Du_{xx} + f(u), & t > 0 \quad x \in (0,1), \\ u_x(0,t) = u_x(1,t) = 0, & t > 0, \\ u(x,0) = u_0(x). \end{cases} \tag{4}$$

The stationary problem associated with (4) can be written as

$$\begin{cases} Du'' + f(u) = 0, \\ u'(0) = u'(1) = 0. \end{cases} \tag{5}$$

where $'$ denotes the derivative with respect to x. This second-order ODE can be transformed into a first-order system, given by:

$$\begin{cases} \dfrac{du}{dx} = \dfrac{1}{D} v, \\ \dfrac{dv}{dx} = -f(u), \end{cases} \tag{6}$$

which is a conservative system with total energy

$$E(u,v) = \frac{v^2}{2D} + F(u)$$

with

$$F(u) := \int_0^u f(s)\,\mathrm{d}s.$$

The stationary solutions of (4) are given by trajectories of system (6) beginning and ending (at "time" 1) on the u axis and thus contained in level curves of $E(u,v)$. Eqs. (6) share the same three equilibrium points of the mean field model, here given by $P_0 = (0,0)$, and the pair $P_\pm = (u_\pm, 0)$, with

$$u_\pm = \frac{1}{2}\left(1 - \theta \pm \sqrt{(\theta-1)^2 - \frac{4\epsilon}{k}}\right). \tag{7}$$

provided that $(1-\theta)^2 > 4\epsilon/k$, (i.e. $\theta < \theta_c$ being θ_c the bifurcation value). The constant functions on $[0,1]$ with values 0, u_- and u_+ are the three (possible) constant stationary solutions of (4). It can be seen that when the discriminant of (7) is zero the fixed points $u_\pm$ collide in a center-saddle bifurcation (see below for the stability conditions). The bifurcation value making the discriminant equal to zero defines a critical value of the habitat degradation parameter (which is the same as the one of the mean field model), given by:

$$\theta_c = 1 - 2\sqrt{\frac{\epsilon}{k}}. \tag{8}$$

That is, the equilibria $P_\pm$ collide when $\theta = \theta_c$. The local stability of the equilibrium points can be computed from $\det|\mathcal{J}(P_{0,\pm}) - \lambda I| = 0$, being $\mathcal{J}$ the Jacobian matrix of Eqs. (6), given by:

$$\mathcal{J} = \begin{pmatrix} 0 & D^{-1} \\ ku(2(\theta-1)+3u) + \epsilon & 0 \end{pmatrix},$$

with eigenvalues

$$\lambda_\pm = \pm\sqrt{D^{-1}(ku(2(\theta-1)+3u)+\epsilon)}.$$

P_0 is a saddle point since $\lambda_\pm(P_0) = \pm\sqrt{\epsilon/D}$. On the other hand, a straightforward computation using (7) gives

$$\lambda_\pm(u_+) = \pm\sqrt{\frac{k}{2D}}\sqrt{\sqrt{(1-\theta)^2 - 4\frac{\epsilon}{k}}\left(1 - \theta + \sqrt{(1-\theta)^2 - 4\frac{\epsilon}{k}}\right)}$$

implying that u_+ is also a saddle, and

$$\lambda_\pm(u_-) = \pm\sqrt{\frac{k}{2D}}\sqrt{\sqrt{(1-\theta)^2 - 4\frac{\epsilon}{k}}\left(1 - \theta - \sqrt{(1-\theta)^2 - 4\frac{\epsilon}{k}}\right)}\ i,$$

which, together with the conservative character of the system, ensures that u_- is a center.

Fig. 2 shows the phase plane (with space as the independent variable) of system (6) for different values of θ. Nonconstant stationary solutions of (4) correspond to trajectories of (6) with initial condition on the u axis (so $v(0) = Du'(0) = 0$) which are part of periodic orbits

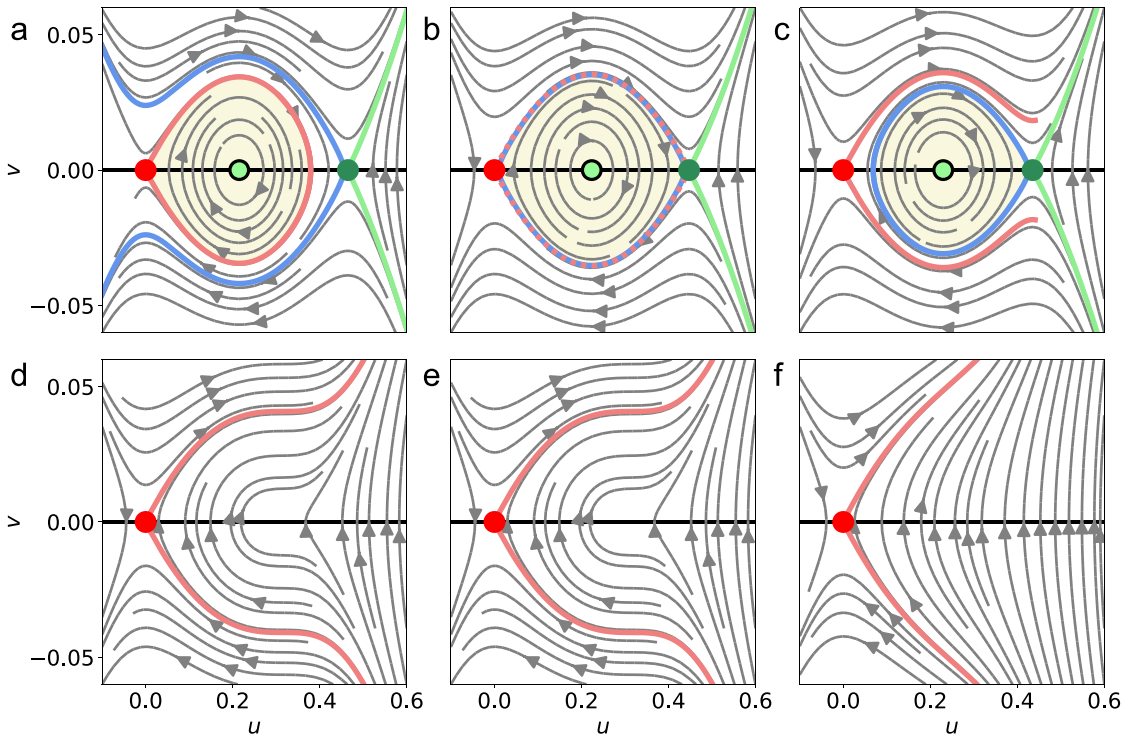

Fig. 2. Dynamics of Eqs. (6) setting $k = 1$, $\epsilon = 0.1$ (with $\theta_c = 0.3675444\cdots$) and: (a) $\theta = 0.32$; (b) $\theta = 0.3291796 = 1 - 3\sqrt{\epsilon/2}$; (c) $1 - 3\sqrt{\epsilon/2} < \theta = 0.335 < 1 - 2\sqrt{\epsilon}$; (d) $\theta = \theta_c$; (e) $\theta = \theta_c + 10^{-6}$; and (f) $\theta = \theta_c + 10^{-1}$. The arrows indicate the direction of the orbits. Big solid dots denote equilibria: saddle points (red and dark green) and center (light green). Here, we show the homoclinic orbit of u_0 (red) in (a); the heteroclinic orbit connecting u_0 and u_+ (dashed red line over blue) in (b); and the homoclinic orbit of u_+ (blue) in (c). Panels (d–f) show the orbits after the s–n bifurcation. (For interpretation of the references to color in this figure legend, the reader is referred to the web version of this article.)

of the center with half period equal to the inverse of a natural number (thus ending at "time" 1 on the u axis, so $v(1) = Du'(1) = 0$). They can only exist for $\theta < \theta_c$ (Fig. 2a–c). Since the boundary of the region of the phase plane where all trajectories are periodic is a homoclinic orbit of one of the saddle points (Figs. 2a,c) or, for a critical value of the parameter, two heteroclinic orbits joining these two saddle points (Fig. 2b), we can always find orbits of periods as long as we want (those that pass close to the saddle points). On the other hand, the periodic orbits close to the center point u_- have a period which tends to $2\pi/\Im(\lambda_+(u_-))$ (see Theorem 9 in [61]).

Hence, the continuity of the period function (see for example [62]) implies that the center will have orbits of any period in the interval $\left(2\pi/\Im(\lambda_+(u_-)), \infty\right)$, guaranteeing the existence of (at least) a number of nonconstant stationary solutions of (6) equal to twice the integer part of $\Im(\lambda_+(u_-))/\pi$ unless this is an integer in which case, the number of nonconstant stationary solutions is two units lower. The fact that there are no more solutions follows from the monotonicity of the period function for our f (see Proposition 3.1 in [63]). The graph of the period function, some trajectories, and the corresponding stationary densities are depicted in Fig. S1.

The study of the equilibria and stability of scalar reaction–diffusion equations has a long history [64–67]. In particular, Chafee showed that any isolated non-constant stationary solution of (4) is unstable [62]. This result was later generalized to higher dimensions in convex domains [68,69]. Thus, the only possible stable steady states of (4) are constant (independent of the spatial position).

Denoting by $\hat{u}$ a constant steady state of (4), the linearization of (2) with Neumann boundary conditions in a neighborhood of $\hat{u}$ is

$$\begin{cases} w_t &= Dw_{xx} + f'(\hat{u})w, \\ w_x(0,t) &= w_x(1,t) = 0. \end{cases} \tag{9}$$

Looking for exponential solutions $w(x,t) = e^{\lambda t}z(x)$, we obtain the following problem for $z(x)$:

$$Dz'' = (\lambda - f'(\hat{u}))z, \quad z'(0) = z'(1) = 0,$$

which implies $\lambda_k = f'(\hat{u}) - k^2 D$, $k = 0, 1....$ Taking into account the sign of f' at the steady states, we obtain that u_0 and u_+ are locally asymptotically stable whereas u_- is unstable. Moreover, for $\theta > \theta_c$, since

$$V(t) = \frac{1}{2}\int_0^1 Du_x^2(x,t)\,\mathrm{d}x - \int_0^1 F(u(x,t))\,\mathrm{d}x$$

is a Lyapunov function of (4) the trivial steady state is globally asymptotically stable (see [65] where the problem with Dirichlet boundary conditions is studied).

Once u_- and u_+ have collided in a saddle–node bifurcation (at $\theta = \theta_c$, involving no equilibria in the PDE except for u_0 for any $\theta > \theta_c$), the flows get curved and spend long times around the v axis. This can be observed in panels (d) and (e) in Fig. 2. When the distance to the bifurcation is large, the flows travel straighter in the phase plane, spending a lower amount of time (Fig. 2f). These changes in the geometry of the vector field may be related to the delays we observe in the spatial system.

In Appendix A.1, we consider the normal forms of (2) with $D = 0$ and $D > 0$ in a neighborhood of the point (θ_c, u_c), understood as an element of the parameter space times the state space, for $\theta > \theta_c$. Here u_c stands for the steady state at the bifurcation, i.e., $u_c = (1 - \theta_c)/2$. More precisely, the rescaling $\hat{t} := (\epsilon k)^{1/4}t$; $\hat{u} := (\epsilon k)^{1/4}(u - u_c)$; and $\mu := \epsilon(\theta - \theta_c)$ (remember that neither ϵ nor k are assumed to be small) transforms Eq. (2) with $D = 0$ into

$$\hat{u}' = -\mu - \hat{u}^2 + O\left(\mu\hat{u}, \hat{u}^3\right)$$

and Eq. (2) with $D > 0$ into

$$\hat{u}_{\hat{t}} = -\mu - \hat{u}^2 + \hat{D}\hat{u}_{xx} + O\left(\mu\hat{u}, \hat{u}^3\right)$$

where $\hat{D} = (\epsilon k)^{-1/4}D$. We obtain bounds of the solution of (2) of the form $\|\hat{u}\|_\infty \leq \sqrt{\mu} + C\mu$, i.e. $\|u - u_c\| \leq (\epsilon k)^{-\frac{1}{4}}\left(\sqrt{\mu} + C\mu\right)$ for a time interval of length of the order of $1/\sqrt{\mu}$ (see Eqs. (24) and (27)), where C depends on how far from a constant function is the

initial condition. Moreover, in (27) the constant C tends to 0 when the diffusion coefficient increases.

Remark 3.1. Standard comparison principles (see e.g. Theorem 4.10 in [66]) guarantee that two solutions to (2) maintain order if they are initially ordered. Therefore, a solution to (2) with initial condition with a minimum value u_m larger or equal (or even slightly smaller) than u_c will "notice" the ghost and thus will behave with an extinction time larger than the one of the homogeneous solution with initial condition u_m.

3.2. PDE model: Numerical results

Here, we illustrate the properties of spatial ghost transients towards extinction by means of numerical simulations of the solutions for the initial value problem (4). The method used to obtain these numerical solutions is described in Appendix A.2. Most of the numerical analyses consider the initial condition $u(x,0) = 0.35 + 0.15\sin(4\pi x)$ (Fig. 3). Since we are also interested in the impact of the initial spatial distribution of the replicators (which may result crucial in cooperative species) other initial conditions are investigated. The solutions for the spatial system indicate that space makes transients not only depend on the distance to the bifurcation value (θ_c), but also on the diffusion coefficient (D), as shown in Fig. 3a. Fixing the fraction of habitat loss right after the bifurcation, transients for large diffusion constants become similar to the ones obtained for the mean-field model, showing the inverse square-root scaling law (Fig. 3b). This is due to the fast homogenization of the system (see the panel on the left in Fig. 3c). Moreover, when diffusion is extremely small the system behaves as an uncoupled lattice showing a heterogeneous extinction pattern (see the mid and right panels in Fig. 3c).

In between these two extremes sharing similar transients' behaviors, there exists a region where transients become much faster and thus the ghost effect is lost. With the initial spatial distribution of cooperators used in Fig. 3, this acceleration in extinction transients is found at $10^{-5} \lesssim D \lesssim 10^{-2.5}$, showing the fastest extinctions times for $D \approx 10^{-3}$. Note that these values of diffusion are not affected by how far the system is from the bifurcation value. It is important to notice that the results obtained for the non-spatial model (dashed line in Fig. 3b) seem to be the upper limit for these transient times, contrarily to some results on spatial ecology showing that space enlarges transients [5,21–23]. Panels in Fig. 3b illustrate some of the extinction dynamics for different values of diffusion, showing the rapid homogenization at large diffusion values and the heterogeneity in population numbers at extremely small diffusion values (see also Fig. S2).

Up to now, we have used a single initial spatial distribution of the species by using a sinusoidal function involving that, in some spatial regions, the population of cooperators is below the bottleneck i.e., the region of the phase space where the saddle and the node collided. This involves that, in such regions, the flows start at population values far away from the ghost thus not being influenced by it (see red arrow in Fig. 3c). That is, our results on diffusion showing shorter transients are found when the population values are below the bottleneck in some spatial regions. When all (or almost) all the population remains above the bottleneck, the ghost effect is recovered, as shown in Fig. S3.

In order to evaluate how general are the results discussed above, we investigate different initial spatial configurations of cooperators. Firstly, we use the same sinusoidal function tuning the ordinary frequency given by ω in $U(x,0) = 0.35 + 0.15\sin(2\pi\omega x)$, as shown in Fig. 4b. For low frequencies, the faster extinction times are found at higher diffusion rates (Fig. 4a) compared to the largest frequencies. Similar results, showing that for intermediate diffusion values extinction transients become faster, have been obtained for random initial populations (see Figs. 5a and Fig. S4c). Here, the $-1/2$ scaling law for extinction times is also found for extremely large and small diffusion rates. The scaling law is lost for $10^{-7} \lesssim D \lesssim 10^{-4}$, where times become much shorter (Fig. 5c). The same qualitative results have been obtained for linear (Fig. S4a), step (Fig. S4b), and high-amplitude sinusoidal (Fig. S4c) functions, for which the values of D displaying the fast extinctions slightly changed. For all these cases, as mentioned above, the transient times never overcame the predictions of the mean-field model for extreme diffusion values, either large or small. Finally, we have evaluated ghost extinction transients under different scenarios where the initial population of cooperators is demoted, simulating a further spatial fragmentation occurring once the threshold of habitat loss has been surpassed. To do so, we have computed extinction times at increasing random gap frequencies (Figs. S5 and S6). Generically, the extinction times decrease at increasing gap frequencies. Despite that for both extreme diffusion values, ghost transients are recovered, the response to this initial spatial fragmentation is shown to be largely asymmetric for these extreme values. For instance, large diffusion values favor long ghost transients with $\theta = \theta_c + 10^{-5}$ (Fig. S5c). The same analyses, showing that for $\theta = \theta_c + 10^{-3}$ ghost transients are faster, are displayed in Fig. S6.

3.3. A two-patch model explains short transients at intermediate diffusion values

We here analyze one of the simplest spatial models for the system previously studied considering a two-compartment, metapopulation model described by ODEs coupled through dispersal (diffusion) see Fig. 6a. This approach is inspired in the classical works by Levin [70], where the study of complex spatial dynamics [71] was simplified by modeling colonization-extinction dynamics among different patches. Our aim here is to shed light on the impact of diffusion in extinction transients by using this simple approach, which reproduces some of the properties identified in the PDE model. That is, that extremely short transients are found for some intermediate diffusion values (see Figs. 3a, 4a, 5a, S4, and S5a). The simplified version of the previous model (2) can be written as:

$$\frac{du_1}{dt} = ku_1^2(1-\theta-u_1) - \epsilon u_1 - D\left(u_1 - u_2\right) \tag{10}$$

$$\frac{du_2}{dt} = ku_2^2(1-\theta-u_2) - \epsilon u_2 - D\left(u_2 - u_1\right), \tag{11}$$

with u_1 and u_2 being the population densities of the autocatalytic species in compartments 1 and 2, respectively. The dynamics of this model without habitat loss ($\theta = 0$) were previously studied [20]. Here, we will focus on the phenomena observed at intermediate diffusion values causing extremely short transients. This is due to the changes in the vector field induced by diffusion rates after the bifurcation (see Fig. 6 and Fig. S8) and even before the bifurcation (Fig. S7). The nullclines are given by

$$\frac{du_1}{dt} = 0 \longrightarrow u_2(u_1) = u_1 - \frac{ku_1^2(1-\theta-u_1) - \epsilon u_1}{D}, \tag{12}$$

$$\frac{du_2}{dt} = 0 \longrightarrow u_1(u_2) = u_2 - \frac{ku_2^2(1-\theta-u_2) - \epsilon u_2}{D}. \tag{13}$$

The crossings between these nullclines determine the equilibrium points, which are found at the origin (where both species become extinct i.e., $u_1 = u_2 = 0$) and the other appear in pairs at the phase plane [20], including those in the diagonal. This means that, depending on the initial conditions, the orbits will be attracted towards the ghost in the diagonal having homogeneous extinction ($u_1 = u_2$) or will pass very close to the axes, involving a delay and a heterogeneous extinction. Given that this system is symmetric, combining both nullclines enables intersections near to the axes (the heterogeneous conditions) provided D is small. The points where the nullclines cross the axes are $u = 0$ and

$$u = u_{\pm} = \frac{1-\theta}{2} \pm \sqrt{\frac{(1-\theta)^2}{4} - \frac{D+\epsilon}{k}}.$$

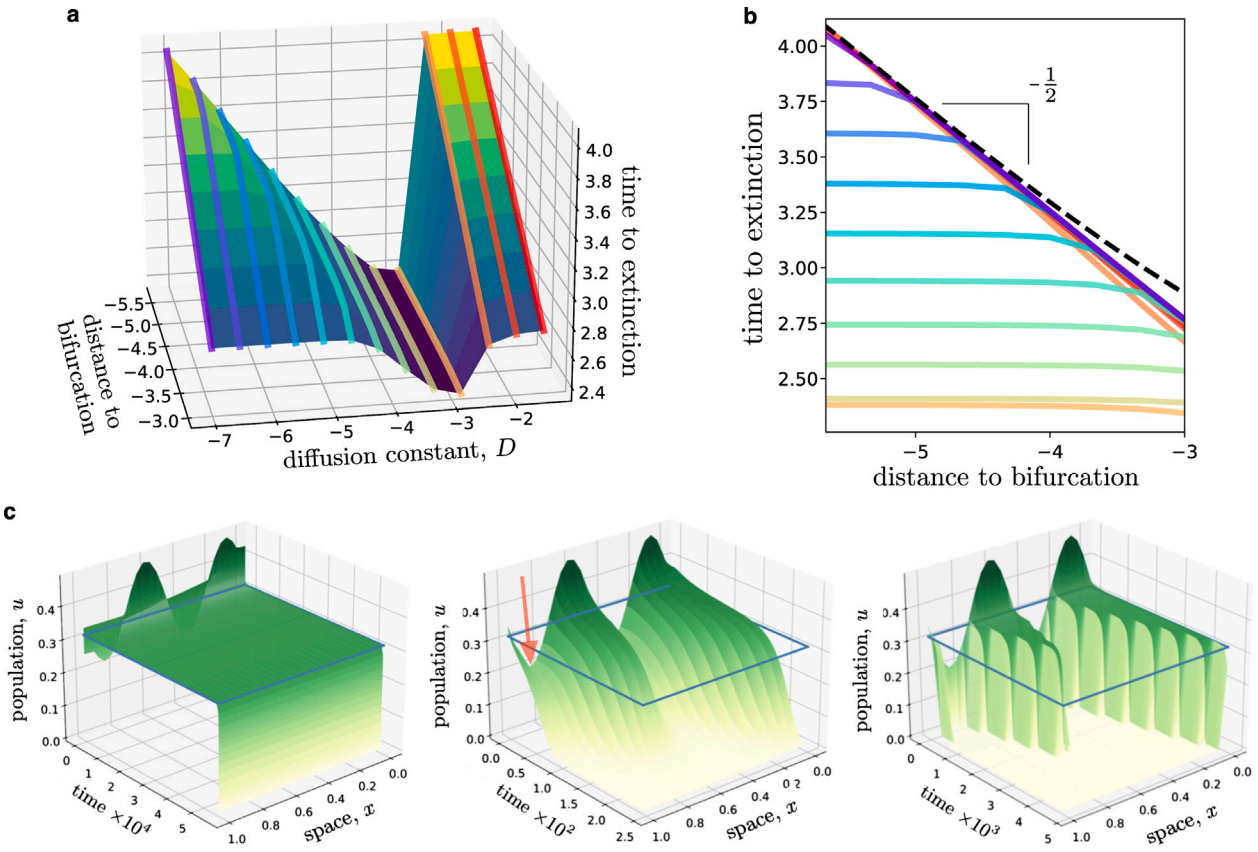

Fig. 3. Ghost delays in continuous space not only depend on the parametric distance to the bifurcation but also on the diffusion rate D. (a) Times to extinction computed in the space $(D, \theta - \theta_c)$ in logarithmic scales. The scaling relations of the extinction time with bifurcation distance are shown in (b) using the values highlighted with the color lines in (a). (c) Extinction time series setting $\theta = \theta_c + 10^{-7}$ for diffusion rates $D = 10^{-2}$ (left); $D = 10^{-4}$ (middle); $D = 10^{-7}$ (right). The blue rectangle in panels (c) indicate the value of u at which the saddle and the node collide in the s–n bifurcation i.e., bottleneck. The red arrow points to a spatial region where the population is below the bottleneck. In all plots we have used $\epsilon = 0.1$ and $u(x, 0) = 0.35 + 0.15\sin(4\pi x)$ as initial spatial distribution of cooperators. (For interpretation of the references to color in this figure legend, the reader is referred to the web version of this article.)

For this model, there will be a s–n bifurcation occurring when the equilibria at the diagonal (homogeneous case) collide, at

$$\theta_c = 1 - 2\sqrt{\frac{\epsilon}{k}},$$

which coincides with the bifurcation value of the mean field model. On the other hand, depending on the diffusion parameter (large D), the nullclines will never be close to the axis, making completely impossible the heterogeneous behavior. This phase plane structure makes it possible to find two bottleneck regions causing extremely long transients: the ghosts from the homogeneous and the heterogeneous case.

Following this simple model, two possible ways of going to extinction can be found: via homogenization of the system and through heterogeneous extinction dynamics (results that remind us of the ones observed for the PDE system, see Fig. 3). As it can be seen in Fig. 6d, diffusion only affects the heterogenizing phenomena by increasing the speed towards global extinction. In this case, increasing diffusion makes the bottleneck that produces the heterogeneous ghost disappear (see Fig. S10). Moreover, for extremely high values of diffusion, the homogenization is rapid enough to capture all the possible initial conditions. This explains why for extreme values of diffusion the system recovers the $-1/2$ scaling law, but, in between there are faster ways to go to extinction depending on the initial conditions (see Fig. S9 and S10). In summary, depending on the initial populations there are three possible extinction scenarios: getting trapped by the homogenizing ghost, getting trapped by the heterogeneous one, or being attracted by both delaying states. This latter condition may produce that some trajectories avoid getting stacked at the ghost making thus trajectories become extinct faster than expected by the $-1/2$ scaling law. However, for particular initial populations where one of the species is just below the bottleneck region and the other one is at larger population values, the orbits could visit two ghosts experiencing longer delays than the one caused by a single bottleneck.

Extrapolating the same results to the continuum model, the same rationale could be behind the phenomena observed during the whole article, for extreme diffusion values all the trajectories get trapped by the homogeneous or heterogeneous ghosts while intermediate diffusion values allow some initial conditions to avoid both ghosts conditions.

4. Conclusions

Since the seminal work by Alan M. Turing on morphogenesis [72], the impact of spatial diffusion in the dynamics of complex biological systems has been an important matter of debate in different fields such as ecology [70,71,73–75], epidemiology [76,77], and origin of life [58,78–81], among others. It is known that spatial correlations can involve the emergence of novel phenomena in nonlinear systems including spatial self-structuring [78,80,82], diffusion-induced chaos [83,84], or resistance of hypercycles to parasites [78,80,85,86]. Mathematical and computational models have also revealed that space typically enlarges transients towards equilibria [5,21–23]. Here, we have addressed a poorly investigated phenomenon. That is, what is the impact of local, spatial correlations in the transients found right after a bifurcation, focusing on the saddle–node (s–n) bifurcation (or, equivalently, close to a first-order phase transition [58]). We have addressed this question by using a one-variable model describing the population dynamics of a self-cooperative (i.e., intra-specifically cooperative or autocatalytic) species. Examples of positive feedback are found in a multitude of

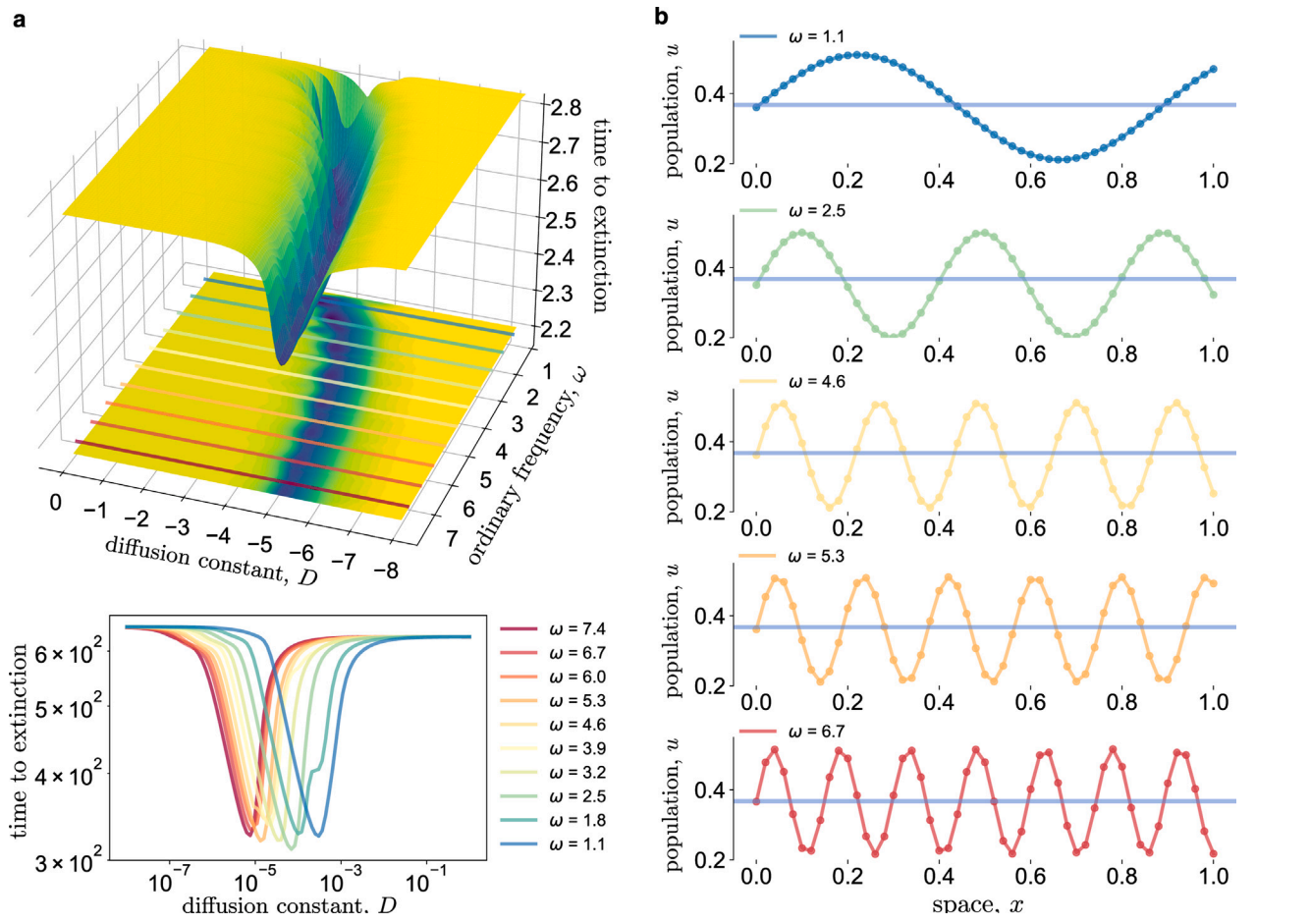

Fig. 4. (a) Time to extinction (in logarithmic scale) for different values of diffusion and initial conditions of the form $U(x,0) = 0.35 + 0.15\sin(2\pi\omega x)$, ω being the ordinary frequency (some examples of these initial conditions are shown in (b) with different colors). The plot below displays how ghost extinction transients change at increasing diffusion (each color corresponds to the values of ω represented with the color lines at the bottom of the 3D plot above and in panel (b)). Here, we use $\theta = \theta_c + 10^{-3}$. (For interpretation of the references to color in this figure legend, the reader is referred to the web version of this article.)

biological systems, including i.a., mechanisms of cancer cells' proliferation [53], reproduction of marine species [52], plants facilitation [43–46], or cooperative dynamics between animals [49–51]. Together with intra-specific cooperation, we have considered intra-specific competition and two processes related to species' survival: habitat loss and decay (see Refs. [38,59] for details on the mean-field dynamics for this system).

The results presented in this article correspond to a species extended and cooperating in a one-dimensional, continuous spatial domain assuming determinism. Mean-field models have revealed that the inverse square-root scaling law is locally found close to a s–n bifurcation, independently of its dimension [25,38,59]. By local, we mean that this scaling law appears tied to the flows starting close to the region of the phase space where the saddle and the node collided: the bottleneck region. Initial conditions far away from this bottleneck in high-dimensional systems give place to anomalies in the scaling law [39,87]. The model studied here presents a s–n bifurcation, and we have focused on transients arising right after the critical fraction of habitat loss is surpassed. The same results may be found using other model parameters as bifurcation parameters. We have focused on a case where the initial amount of population is spatially-heterogeneous and jeopardized in some places, mimicking an endangered ecosystem in which the density of the species is below the bottleneck in some spatial regions.

We have found that for extreme values of diffusion, both large and small, the system as a whole is able to get trapped into the bottleneck of the ghost, and the inverse square-root scaling law is found. However, for intermediate values of diffusion, transients become faster and the species rapidly extinct. That is, despite some of the spatial regions having population values that may be locally captured by the ghost bottleneck, the whole population do not experience the delayed transition. These results have been found robust for a multitude of different initial spatial distributions of cooperators, and we have introduced a simple two-patch metapopulation model also capturing these dynamics found at intermediate diffusion values. Together with the reaction–diffusion model, we have provided multitude of numerical evidence for this phenomenon making transients faster and thus accelerating extinctions at intermediate diffusion values. The theoretical basis explaining this effect remains an open question that should be addressed in the future.

We have identified different mechanisms behind extinction transients in the metapopulation model, one of them involving passing close to two bottleneck regions. The idea of the concatenation of ghosts was recently proposed in Ref. [8]. We emphasize that these concatenations could be a new mechanism behind supertransients [57], beyond the other mechanisms discussed in the introduction e.g., varying time scales, stochasticity, etc. This topic should be investigated in future research using simple models (or normal forms) having two or more ghost bottlenecks influencing the orbits. Finally, we have provided estimates of the extinction times for the studied model transformed into a spatially-explicit, normal form for the s–n bifurcation.

Finally, we want to emphasize that the spatial bifurcation value does not depend on diffusion and that the results obtained for the non-spatial model (see e.g., the dashed line in Fig. 3b) seem to be the upper limit for these transient times, contrarily to some results

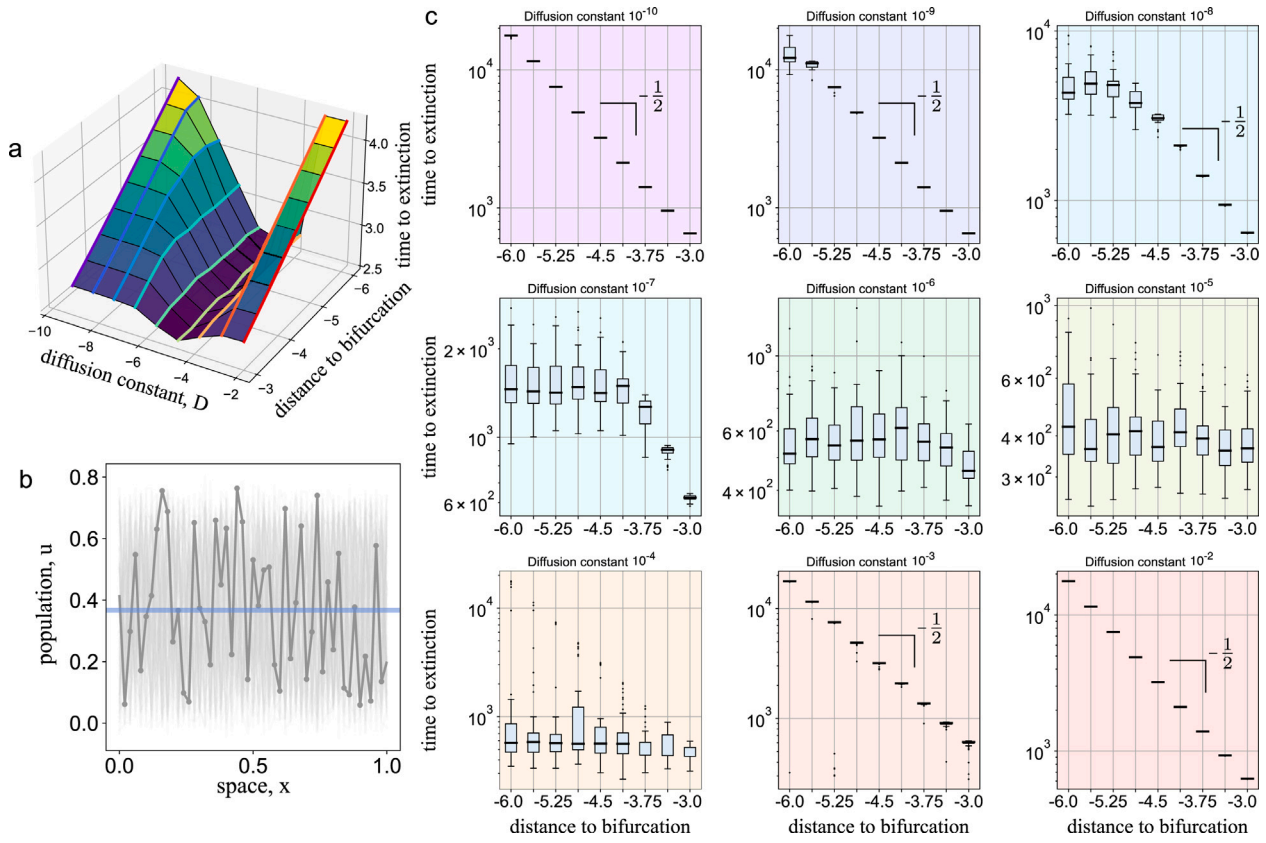

Fig. 5. (a) Mean extinction times of the whole population depending on the distance to the bifurcation and the diffusion constant (in triple logarithmic scale). The results are obtained from an ensemble of 10^2 random initial conditions (gray lines), with population densities $U(x,0)$ distributed uniformly around the bottleneck (blue line) (b). (c) Box plots showing how all of the realizations are distributed depending on their distance to the bifurcation. Even with this ensemble of random initial conditions, the scaling law is recovered in the diffusion extremes (either large $D > 10^{-3}$ or small $D < 10^{-9}$). In the other cases, saturation or even a complete insensitivity to the parameter value can be observed. (For interpretation of the references to color in this figure legend, the reader is referred to the web version of this article.)

on spatial ecology showing that space makes transients longer [5,21–23]. It would be interesting to see if this is a universal property for other bifurcations, both local and global. Moreover, recent research has focused on the impact of intrinsic noise in the statistics of ghost transients and the associated scaling laws for the mean extinction times, $\bar{T}$ right after the stochastic s–n bifurcations. Such investigations have revealed that (i) ghosts remain robust to demographic fluctuations, (ii) the length of the transients increases at increasing noise levels (decreasing the system's size), (iii) the scaling law for $\bar{T}$ follows more complex functions than simple power laws [42]. As mentioned, we here have restricted to a spatial, deterministic approach. Future research should also investigate the interplay between space and demographic fluctuations in the properties of ghost transients and scaling.

CRediT authorship contribution statement

Àngel Calsina: Performed the analytical calculations, Numerical simulations, Analyzed the models and data, Writing of the manuscript and in the revision process. **Sílvia Cuadrado:** Performed the analytical calculations, Analyzed the models and data, Writing of the manuscript and in the revision process. **Blai Vidiella:** Performed the analytical calculations, Numerical simulations, Analyzed the models and data, Writing of the manuscript and in the revision process. **Josep Sardanyés:** Conceived the mathematical model, Performed the analytical calculations, Analyzed the models and data, Writing of the manuscript and in the revision process.

Declaration of competing interest

The authors declare no conflict of ineterest.

Data availability

No data was used for the research described in the article.

Acknowledgments

This research has been funded through the 2020–2021 Biodiversa and Water JPI joint call under the BiodivRestore ERA-NET Cofund (GA N° 101003777) project MPA4Sustainability with funding organizations: Innovation Fund Denmark (IFD), Agence Nationale de la Recherche (ANR), Fundação para a Ciência e a Tecnologia (FCT), Swedish Environmental Protection Agency (SEPA) and grant PCI2022-132926 funded by MCIN/AEI/10.13039/501100011033 and by the European Union NextGenerationEU/PRTR (J.S. and B.V). This work is also supported by the Spanish State Research Agency, through the Severo Ochoa and María de Maeztu Program for Centers and Units of Excellence in R&D (CEX2020-001084-M). We thank CERCA Programme/Generalitat de Catalunya for institutional support. J.S. has been also supported by the Ramón *y* Cajal grant RYC-2017-22243 funded by MCIN/AEI/10.13039/501100011033 "FSE invests in your future", as well as by grant PID2021-127896OB-I00 funded by MCIN/AEI/10.13039/501100011033 "ERDF A way of making Europe". B.V. has been also funded by grant RYC-2017-22243, whose PI is J.S. A.C. and S.C. have been supported by grants MTM2017-84214-C2-2-P, RED2018-102650-T, and PID2021-123733NB-I00 funded by MCIN/AEI/10.13039/501100011033 "ERDF A way of making Europe".

Appendix A

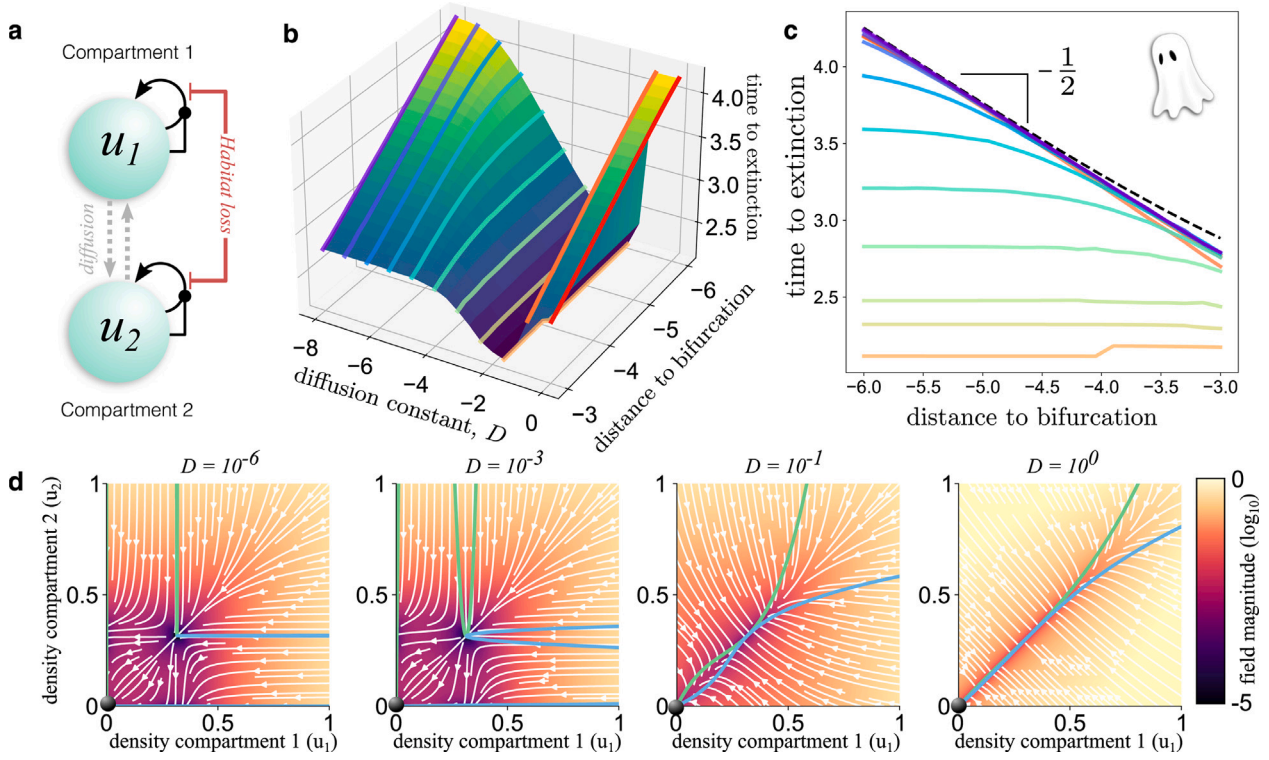

Fig. 6. (a) Schematic representation of the two compartments model studied in Section 3.3. (b) Dependence of times to extinction on diffusion rate and the distance to the bifurcation. (c) Changes in the scaling law for the diffusion values shown in panel (b) using the same line colours. For intermediate diffusion rates, the extinction becomes much faster than in both extremes. (d) Phase portraits for different diffusion rates close to bifurcation with $\theta = \theta_c + 10^{-8}$. Here, the flow is displayed with white arrows, and the nullclines with green [Eq. (12)] and blue [Eq. (13)] lines. The black marble denotes the only stable fixed point. For panels (b) and (c) the initial condition chosen is $u_1 = 0.1$ and $u_2 = 0.65$. (For interpretation of the references to color in this figure legend, the reader is referred to the web version of this article.)

A.1. Spatial normal form: transients' scaling

We start by reducing Eq. (2) to its normal form. Let us remind that $\theta_c = 1-2(\epsilon/k)^{1/2}$. This gives $u_c = (1-\theta_c)/2 = (\epsilon/k)^{1/2}$. Now we introduce the rescaling $\hat{t} = (\epsilon k)^{1/4}t, \hat{u} = (\epsilon k)^{1/4}(u-u_c)$ and rename $\mu = \epsilon(\theta-\theta_c)$ and $\hat{D} = (\epsilon k)^{-1/4}D$. We have

$$u = u_c + (\epsilon k)^{-1/4}\hat{u} = (\frac{\epsilon}{k})^{1/2} + (\epsilon k)^{-1/4}\hat{u} \tag{14}$$

and

$$\theta = \theta_c + \mu/\epsilon = 1 - 2(\frac{\epsilon}{k})^{1/2} + \mu/\epsilon.$$

Then, we can write

$$1-\theta-u = \left(\frac{\epsilon}{k}\right)^{1/2} - \frac{\mu}{\epsilon} - (\epsilon k)^{-1/4}\hat{u}$$

and

$$u^2 = \frac{\epsilon}{k} + 2\epsilon^{1/4}k^{-3/4}\hat{u} + (\epsilon k)^{-1/2}\hat{u}^2.$$

Hence,

$$k(1-\theta-u)u^2 = k\left(\left(\frac{\epsilon}{k}\right)^{3/2} + 2\epsilon^{3/4}k^{-5/4}\hat{u} + k^{-1}\hat{u}^2 - \frac{\mu}{k} - \epsilon^{3/4}k^{-5/4}\hat{u} - 2k^{-1}\hat{u}^2 + O(\mu\hat{u},\hat{u}^3)\right),$$

and

$$k(1-\theta-u)u^2 - \epsilon u = \epsilon^{3/2}k^{-1/2} + \epsilon^{3/4}k^{-1/4}\hat{u} - \mu - \hat{u}^2 + O(\mu\hat{u},\hat{u}^3) - \epsilon\left((\frac{\epsilon}{k})^{1/2} + (\epsilon k)^{-1/4}\hat{u}\right) = -\mu - \hat{u}^2 + O(\mu\hat{u},\hat{u}^3).$$

On the other hand,

$$\frac{du}{dt} = \frac{d}{d\hat{t}}(u_c + (\epsilon k)^{-1/4}\hat{u})\frac{d\hat{t}}{dt} = (\epsilon k)^{-1/4}\frac{d\hat{u}}{d\hat{t}}(\epsilon k)^{1/4} = \frac{d\hat{u}}{d\hat{t}},$$

and, for the diffusion operator,

$$D\frac{\partial^2 u}{\partial x^2} = (\epsilon k)^{-1/4}D\frac{\partial^2\hat{u}}{\partial x^2} = \hat{D}\frac{\partial^2\hat{u}}{\partial x^2}.$$

Therefore Eq. (2) transforms in

$$\hat{u}_{\hat{t}} = -\mu - \hat{u}^2 + \hat{D}\hat{u}_{xx} + O(\mu\hat{u},\hat{u}^3).$$

Next, we study the normal form of the equation to exemplify the behavior of the solutions close and above to the bifurcation value of the parameter i.e., when the model equation has no coexistence equilibrium. Notice that we suppress the hats in the following to simplify notation.

To begin with, and before adding the diffusion operator, we have the following ODE which is the normal form of the saddle–node (s–n) bifurcation,

$$u'(t) = -\mu - u(t)^2$$

for small $\mu > 0$, implying that $u = 0$ is near to an equilibrium point (a "ghost" equilibrium). In the following, we will consider $u^0 > 0$ as fixed and obtain estimates which depend on μ. The equation above can be explicitly solved for an initial condition $u(0) = u^0$, giving

$$\tilde{u}(t) = \sqrt{\mu}\tan\left(\arctan\left(\frac{u^0}{\sqrt{\mu}}\right) - \sqrt{\mu}\,t\right), \quad t \in (t_1, t_2),$$

where

$$t_1 := \frac{1}{\sqrt{\mu}}\left(\arctan\left(\frac{u^0}{\sqrt{\mu}}\right) - \frac{\pi}{2}\right) < 0$$

$$< t_2 := \frac{1}{\sqrt{\mu}}\left(\arctan\left(\frac{u^0}{\sqrt{\mu}}\right) + \frac{\pi}{2}\right).$$

Alternatively one can isolate t as a function of u and u^0 as

$$\tau(u,u^0,\mu) := \frac{\arctan\left(\frac{u^0}{\sqrt{\mu}}\right) - \arctan\left(\frac{u}{\sqrt{\mu}}\right)}{\sqrt{\mu}}$$

which gives the time needed to travel from u^0 to $-u^0$

$$\tau(-u^0,u^0,\mu) = 2\frac{\arctan\left(\frac{u^0}{\sqrt{\mu}}\right)}{\sqrt{\mu}},$$

which is twice the time needed to go from u^0 to the origin. Moreover, $\tilde{u}$ vanishes at

$$\bar{t} = \frac{\arctan\left(\frac{u^0}{\sqrt{\mu}}\right)}{\sqrt{\mu}}$$

and $\tilde{u}(\bar{t}+s) = -\tilde{u}(\bar{t}-s)$, as can be seen by direct substitution.

We define the delay time as the leading term in the expansion of the function $\tau(-u^0,u^0,\mu)$ around $\mu = 0$ which is $\frac{\pi}{\sqrt{\mu}}$ (see [36]). More precisely, $\tau(-u^0,u^0,\mu) = \frac{\pi}{\sqrt{\mu}} - \frac{2}{u^0} + \frac{2\mu}{3(u^0)^3} + O(\mu^2)$. On the other hand, since $\tilde{u}$ is decreasing and an odd function with respect to $\bar{t}$ we have,

$$\begin{aligned}|\tilde{u}(t)| \le \tilde{u}\left(\frac{\bar{t}}{2}\right) &= \sqrt{\mu}\tan\left(\frac{1}{2}\arctan\left(\frac{u^0}{\sqrt{\mu}}\right)\right)\\ &= \frac{u^0}{\sqrt{\frac{(u^0)^2}{\mu}+1}+1} = \frac{\sqrt{\mu}}{\sqrt{1+\frac{\mu}{(u^0)^2}}+\sqrt{\frac{\mu}{(u^0)^2}}} \le \sqrt{\mu}\cdot\min\left(1,\frac{u^0}{2\sqrt{\mu}}\right)\end{aligned} \tag{15}$$

on the (restricted) interval $\left(\frac{\bar{t}}{2},\frac{3}{2}\bar{t}\right)$, where we have used $\tan(\frac{\alpha}{2}) = \frac{\tan\alpha}{1+\sqrt{1+\tan^2\alpha}}$.

We now consider the initial value problem for the reaction–diffusion version of the above ODE with Neumann boundary conditions on the interval $(0,1)$ and an initial condition $u(x,0)$ that we write $u(x,0) = u^0 + v(x)$.

$$\begin{aligned}&u_t(x,t) = -\mu - u(x,t)^2 + Du_{xx}(x,t),\\ &u_x(0,t) = u_x(1,t) = 0,\\ &u(x,0) = u^0 + v^0(x).\end{aligned} \tag{16}$$

We will obtain estimates on the solution of (16) of the form $\sqrt{\mu}+C\mu$ valid for a time interval of length $\bar{t}$, of the order $1/\sqrt{\mu}$ as we already know. In the first one, (24), C depends on u^0 and the sup norm of v^0. The second one, (27), is finer because it exploits the fact that, given $u(x,0)$, u^0 can be taken as the integral of $u(x,0)$ in such a way that the integral of $v^0(x)$ vanishes, C depends on the L^2 norm of the derivative of $v^0(x)$ and it is of the order of 1 over the diffusion coefficient D. For example, Fig. 3 and Fig. S2 show that only diffusion coefficients relatively large ($D \sim 10^{-2}, 10^{-3}$) allow to "see" the ghost equilibrium as predicted by (27).

Let $\tilde{u}$ still denote the solution of the ODE with initial condition u^0. Notice that then $v(x,t) := u(x,t) - \tilde{u}(t)$ solves the problem

$$\begin{aligned}&v_t(x,t) = -2\tilde{u}(t)v(x,t) - v(x,t)^2 + Dv_{xx}(x,t),\\ &v_x(0,t) = v_x(1,t) = 0,\\ &v(x,0) = v^0(x).\end{aligned} \tag{17}$$

Let us denote $g(t) := e^{-2\int_0^t \tilde{u}(s)ds}$. Notice that $g(t)$ has a unique minimum at $t = \bar{t}$ and that $g(\bar{t}+s) = g(\bar{t}-s)$. Moreover, a straightforward computation gives an explicit form for $g(t)$, namely,

$$g(t) = \frac{\mu}{\mu+(u^0)^2}\left(1+\left(\tan\left(\arctan\left(\frac{u^0}{\sqrt{\mu}}\right)-\sqrt{\mu}\,t\right)\right)^2\right).$$

Hence, the following bound holds on the interval $\left(\frac{\bar{t}}{2},\frac{3}{2}\bar{t}\right)$

$$\begin{aligned}0 < g(t) < g(\tfrac{\bar{t}}{2}) &= \frac{\mu}{\mu+(u^0)^2}\left(1+\left(\tan\left(\frac{1}{2}\arctan\left(\frac{u^0}{\sqrt{\mu}}\right)\right)\right)^2\right)\\ &= \frac{2\mu}{(u^0)^2+\mu+\sqrt{\mu}\sqrt{(u^0)^2+\mu}} < \min\left(\frac{2\mu}{(u^0)^2},1\right),\end{aligned} \tag{18}$$

where we used the trigonometric identity

$$\tan^2\left(\frac{\alpha}{2}\right) = \frac{\sqrt{\tan^2\alpha+1}-1}{\sqrt{\tan^2\alpha+1}+1}.$$

Moreover, it is also possible to write explicitly $\int_0^t g(s)ds$, which will be useful later

$$\int_0^t g(s)ds = \frac{u^0 - \sqrt{\mu}\tan\left(\arctan\left(\frac{u^0}{\sqrt{\mu}}\right)-\sqrt{\mu}\,t\right)}{(u^0)^2+\mu}$$

providing the bound

$$\begin{aligned}\int_0^t g(s)ds &\le \int_0^{\frac{3}{2}\bar{t}} g(s)ds = \frac{u^0+\sqrt{\mu}\tan\left(\frac{1}{2}\arctan(\frac{u^0}{\sqrt{\mu}})\right)}{(u^0)^2+\mu}\\ &= \frac{1}{u^0}\left(1-\frac{1}{\sqrt{\frac{(u^0)^2}{\mu}+1}}\right)\left(1+\frac{2}{\sqrt{\frac{(u^0)^2}{\mu}+1}}\right) \le \frac{9}{8u^0}\end{aligned} \tag{19}$$

for $t \in [0,\frac{3}{2}\bar{t})$, which follows from an application of the formula for $\tan(\frac{\alpha}{2})$ and a direct computation of the maximum value of the expression before the last inequality as a function of μ.

On the other hand, $w(x,t) := e^{2\int_0^t \tilde{u}(s)ds}v(x,t) = \frac{v(x,t)}{g(t)}$ fulfills

$$\begin{aligned}&w_t(x,t) = Dw_{xx}(x,t) - g(t)w(x,t)^2,\\ &w_x(0,t) = w_x(1,t) = 0,\\ &w(x,0) = v^0(x)\end{aligned} \tag{20}$$

and so it is the solution of the integral equation (the variation of constants equation)

$$w(x,t) = \big(T(t)v^0\big)(x) - \int_0^t \big(T(t-s)g(s)w(\cdot,s)^2\big)(x)ds, \tag{21}$$

where $T(t)$ stands for the solution semigroup of the (linear) diffusion equation with diffusion coefficient D and with homogeneous Neumann boundary conditions on the interval $(0,1)$.

Let $\|\cdot\|_\infty$ denote the sup norm in the Banach space of the continuous functions on $[0,1]$. $T(t)$ is given in terms of the Fourier series as

$$\big(T(t)z\big)(x) = \sum_{k=0}^{\infty} e^{-Dk^2\pi^2 t}z_k\cos(k\pi x), \tag{22}$$

where $z_0 = \int_0^1 z(x)dx$ and $z_k = 2\int_0^1 z(x)\cos(k\pi x)dx$ for $k = 1,2,\dots$ $T(t)$ is contractive in the space of continuous functions by the maximum principle, in fact, $\|T(t)\| = 1$ (see [88]).

Let us assume $\|v^0\|_\infty < \alpha\exp\left(-\frac{9\alpha}{8u^0}\right)$ for some $\alpha > 0$ to be chosen later. Going back to (21), we have, as long as $\|w(\cdot,s)\|_\infty \le \alpha$ for any $s \in [0,t)$,

$$\begin{aligned}\|w(\cdot,t)\|_\infty &\le \|v^0\|_\infty + \int_0^t g(s)\|w(\cdot,s)^2\|_\infty ds \le \|v^0\|_\infty\\ &+ \int_0^t \alpha g(s)\|w(\cdot,s)\|_\infty ds\end{aligned}$$

which, using Gronwall's inequality and (19) yields

$$\|w(\cdot,t)\|_\infty \le \|v^0\|_\infty e^{\alpha\int_0^t g(s)ds} \le \|v^0\|_\infty\exp\left(\frac{9\alpha}{8u^0}\right) < \alpha \tag{23}$$

for $t \in [0,\frac{3}{2}\bar{t})$ as long as $\|w(\cdot,s)\|_\infty \le \alpha$ for any $s \in [0,t)$. In fact, the inequality $\|w(\cdot,s)\|_\infty \le \alpha$ turns out to hold on the whole time interval $[0,\frac{3}{2}\bar{t})$ and so (23) holds on $[0,\frac{3}{2}\bar{t})$. Indeed, notice that $\|w(\cdot,0)\|_\infty = \|v^0\|_\infty < \alpha$ which implies the existence of a maximal positive $\tilde{t} \le \frac{3}{2}\bar{t}$ such that $\|w(\cdot,t)\|_\infty < \alpha$ for $t \in [0,\tilde{t})$. If $\tilde{t}$ were strictly less than $\frac{3}{2}\bar{t}$, then $\|w(\cdot,\tilde{t})\|_\infty$ would be equal to α contradicting (23).

Note that the best choice of α is $\frac{8}{9}u^0$ for which, $\alpha\exp(-\frac{9\alpha}{8u^0}) = \frac{8}{9e}u^0$. Thus, assuming $\|v^0\|_\infty < \frac{8}{9e}u^0$, and using (18) and (23) (with $\alpha = \frac{8}{9}u^0$), we get the following inequality for the solution of (16) on the interval $(\frac{\bar t}{2}, \frac{3}{2}\bar t)$:

$$\|u(\cdot,t)-\tilde u(t)\|_\infty = \|v(\cdot,t)\|_\infty = g(t)\|w(\cdot,t)\|_\infty \le \frac{2\mu\, e}{(u^0)^2}\|v^0\|_\infty,$$

and, also, using $\|v^0\|_\infty < \frac{8}{9e}u^0$,

$$\|u(\cdot,t)-\tilde u(t)\|_\infty \le \frac{16\mu}{9u^0}.$$

Finally, using (15) we obtain for the solution of the reaction–diffusion problem (16) where we assume $\|v^0\|_\infty < \frac{8}{9e}u^0$, the following bound

$$\|u(\cdot,t)\|_\infty \le |\tilde u(t)| + \|u(\cdot,t)-\tilde u(t)\|_\infty \le \sqrt{\mu} + \frac{2\,e\,\|v^0\|_\infty}{(u^0)^2}\,\mu \tag{24}$$

on the time interval $(\frac{\bar t}{2}, \frac{3}{2}\bar t)$ which is of length $\bar t \approx \frac{\pi}{2\sqrt{\mu}}$.

The above estimates do not make use of the fact that, given an initial condition $u(x,0)$ we can always take $u^0 = \int_0^1 u(x,0)dx$ and thus $\int_0^1 v^0(x)dx = 0$. Taking advantage of this, which implies that the first Fourier coefficient of v^0 vanishes, alternatively we would have, from (22),

$$\begin{aligned}\big(T(t)v^0\big)(x) &= \sum_{k=1}^{\infty} e^{-Dk^2\pi^2 t} v_k \cos(k\pi x)\\ &= e^{-\pi^2 D t}\sum_{k=1}^{\infty} e^{-D(k^2-1)\pi^2 t} v_k\cos(k\pi x),\end{aligned}$$

which allows to bound, using Schwartz inequality and Parseval identity,

$$\begin{aligned}&|\big(T(t)v^0\big)(x)| \le e^{-\pi^2 D t}\textstyle\sum_{k=1}^{\infty}|v_k|\\ &= e^{-\pi^2 D t}\textstyle\sum_{k=1}^{\infty} k|v_k|\,\frac{1}{k} \le e^{-\pi^2 D t}\Big(\sum_{k=1}^{\infty}k^2|v_k|^2\ \sum_{k=1}^{\infty}\frac{1}{k^2}\Big)^{\frac12}\\ &= e^{-\pi^2 D t}\,\tfrac{\pi}{\sqrt6}\|(v^0)'\|_{L^2}.\end{aligned} \tag{25}$$

For any $\alpha > 0$, as long as $\|w(\cdot,s)\|_\infty \le \alpha$ for any $s \in [0,t)$, we will have, using (21),

$$\|w(\cdot,t)\|_\infty \le \frac{\pi}{\sqrt6}\|(v^0)'\|_{L^2}e^{-\pi^2 D t} + \int_0^t \alpha g(s)\|w(\cdot,s)\|_\infty ds,$$

and, by Gronwall's inequality,

$$\|w(\cdot,t)\|_\infty \le \frac{\pi}{\sqrt6}\|(v^0)'\|_{L^2}\left(e^{-\pi^2 D t} + \int_0^t e^{-\pi^2 D s}\alpha g(s)e^{\alpha\int_s^t g(\sigma)d\sigma}ds\right).$$

Using $g(s) \le 1$ and (19), this implies

$$\|w(\cdot,t)\|_\infty \le \frac{\pi}{\sqrt6}\|(v^0)'\|_{L^2}\left(e^{-\pi^2 D t} + \frac{\alpha e^{\frac{9\alpha}{8u^0}}}{\pi^2 D}\left(1-e^{-\pi^2 D t}\right)\right) \tag{26}$$

for $t \in [0, \frac{3}{2}t)$ provided that $\|w(\cdot,t)\|_\infty \le \alpha$ for any $s \in [0,t)$. We fix D_0 and choose α such that $\frac{\alpha e^{\frac{9\alpha}{8u^0}}}{\pi^2 D_0} = 1$. Then the right hand side of the previous inequality is a decreasing function of t whenever $D \ge D_0$.

Further assume $\frac{\pi}{\sqrt6}\|(v^0)'\|_{L^2} < \alpha$ which implies, by the Poincaré–Wirtinger inequality (or by applying (25) with $t = 0$), $\|v^0\|_\infty < \alpha$. Then, an analogous argument to the one above gives that $\|w(\cdot,t)\|_\infty \le \alpha$ holds on the whole interval $[0, \frac{3}{2}\bar t)$ and therefore (26) too.

Finally, we can state: let $D_0 > 0$ be fixed and $\alpha > 0$ be such that

$$\frac{\alpha e^{\frac{9\alpha}{8u^0}}}{\pi^2 D_0} = 1$$

(α can be given explicitly in terms of the Lambert function W as $\alpha = \frac{8}{9}u^0\,W(\frac{9}{8}\frac{\pi^2 D}{u^0})$). Let us assume $\frac{\pi}{\sqrt6}\|(v^0)'\|_{L^2} \le \alpha$ and $D \ge D_0$.

Then on the interval $(\frac12\bar t, \frac32\bar t)$ we have, from (26),

$$\|w(\cdot,t)\|_\infty \le \frac{\pi}{\sqrt6}\|(v^0)'\|_{L^2}\left(\frac{D_0}{D} + \left(1-\frac{D_0}{D}\right)e^{-\pi^2 D t}\right),$$

and, using (18),

$$\begin{aligned}\|u(\cdot,t)-\tilde u(t)\|_\infty &= \|v(\cdot,t)\|_\infty = g(t)\|w(\cdot,t)\|_\infty\\ &\le \frac{\pi}{\sqrt6}\frac{2\mu}{(u^0)^2}\left(\frac{D_0}{D} + \left(1-\frac{D_0}{D}\right)e^{-\pi^2 D t}\right)\|(v^0)'\|_{L^2},\end{aligned}$$

and, as above,

$$\begin{aligned}\|u(\cdot,t)\|_\infty &\le |\tilde u(t)| + \|u(\cdot,t)-\tilde u(t)\|_\infty\\ &\le \sqrt{\mu} + \frac{2\,\pi}{\sqrt6\,(u^0)^2}\left(\frac{D_0}{D} + \left(1-\frac{D_0}{D}\right)e^{-\pi^2 D t}\right)\|(v^0)'\|_{L^2}\,\mu.\end{aligned}$$

$$\begin{aligned}\|u(\cdot,t)\|_\infty &\le |\tilde u(t)| + \|u(\cdot,t)-\tilde u(t)\|_\infty\\ &\le \sqrt{\mu} + \tfrac{2\,\pi}{\sqrt6\,(u^0)^2}\left(\tfrac{D_0}{D} + \left(1-\tfrac{D_0}{D}\right)e^{-\pi^2 D t}\right)\|(v^0)'\|_{L^2}\,\mu\\ &\le \sqrt{\mu} + \tfrac{2\,\pi}{\sqrt6\,(u^0)^2}\left(\tfrac{D_0}{D} + \left(1-\tfrac{D_0}{D}\right)e^{-\pi^2 D \frac{\bar t}{2}}\right)\|(v^0)'\|_{L^2}\,\mu,\end{aligned} \tag{27}$$

where

$$\bar t = \frac{\arctan\frac{u^0}{\sqrt{\mu}}}{\sqrt{\mu}} \approx \frac{\pi}{2\sqrt{\mu}}.$$

A.2. Numerical methods

The computation of the time solutions of the reaction–diffusion system has been performed by means of a semi-implicit, finite differences scheme based on the Crank–Nicolson method for the linear term and an explicit choice for the nonlinear one, given by

$$-\frac{\alpha}{2}u_{n-1}^{m+1} + (1+\alpha)u_n^{m+1} - \frac{\alpha}{2}u_{n+1}^{m+1} = \frac{\alpha}{2}u_{n-1}^{m} + (1-\alpha)u_n^{m} + \frac{\alpha}{2}u_{n+1}^{m} + f(u_n^m),$$

where $\alpha = Ddt/dx^2$ (here dt and dx stand for time and space step sizes, respectively). This has the advantage that avoids the repeated use of Newton (or another) method to solve nonlinear systems of equations while keeping stability even with large time steps. The need to use a (relatively) inexpensive method in computer time and of large time steps comes from the fact that we are interested in very large times, especially when the *ghost equilibrium* is *noticed* by the solution of the partial differential equation.

Moreover, the algorithm uses an adaptive time step method which enlarges its length when the change of the solution (in the L^1 norm in a time step) is small while reduces its length when the change of the solution in a time step is too large. This adaptive time stepping plays an important role in reducing the computer time since the solution typically behaves rapidly at the beginning of the computation (when the diffusion operator acts on a nonhomogeneous density), slowly when an already more or less homogeneous density passes in the vicinity of a *ghost*, and again very rapidly when it is far from it.

Appendix B. Supplementary data

Supplementary material related to this article can be found online at https://doi.org/10.1016/j.chaos.2022.112915.

References

[1] Cushing JM, Dennins B, Desharnais RA, Constantino RF. Moving toward an unstable equilibrium: saddle nodes in population systems. J Anim Ecol 1998;67:298–306.
[2] Hastings A. Transients: the key to long-term ecological understanding? Trends Ecol Evol 2004;19(1):39–45.
[3] Chen X, Joel E. Transient dynamics and food-web complexity in the Lotka–Volterra cascade model. Proc R Soc Lond B 2001;268:869–77.
[4] Hastings A, Abbott K, Cuddington K, Francis T, Gellner G, Lai Y-C, et al. Transient phenomena in ecology. Science 2018;361:eaat6412.
[5] Saravia LA, Ruxton GD, Coviella CE. The importance of transients' dynamics in spatially extended populations. Proc R Soc Lond B 2000;267:1781–6.

[6] Sardanyés J, Duarte J, Januário C, Martins N. Controlling delayed transitions with applications to prevent single species extinctions. Adv Diff Eq Control Proc 2011;10(1):29–41.
[7] Vidiella B, Sardanyés J, Solé R. Exploiting delayed transitions to sustain semiarid ecosystems after catastrophic shifts. J Roy Soc Interface 2018;15:20180083.
[8] Vidiella B, Fontich E, Valverde S, Sardanyés J. Habitat loss causes long extinction transients in small trophic chains. Theor Ecol 2021;14:641–61.
[9] Rinaldi S, Scheffer M. Geometric analysis of ecological models with slow and fast processes. Ecosystems 2000;3:507–21.
[10] Rinaldi S, Muratori S. Limit-cycles in slow-fast forest pest models. Theor Pop Bio 1992;41:315–32.
[11] Finknstadt BF, Grenfell BT. Time series modelling of childhood disease: a dynamical systems appraoch. J R Stat Soc Ser C 2000;49:187–205.
[12] Ludwig D. Qualitative analysis of insect outbreak systems: the spruce budworm and forest. J Anim Ecol 1978;47:315–31.
[13] Chiralt C, Ferragut A, Gasull A, Vindel P. Quantitative analysis of competition models. Nonlin Analys: Real World Appl 2017;38:327–47.
[14] Bulmer M. Theoretical evolutionary ecology. Sinauer; 1994.
[15] McCann K, Yodzis P. Nonlinear dynamics and population disappearances. Am Nat 1994;144:873–9.
[16] Vandermeer J, Yodzis P. Basin boundary collision as a model of discontinuous change in ecosystems. Ecology 1999;80:1817–27.
[17] McCann K, Yodzis P. Bifurcation structure of a three-species food-chain model. Theor Pop Biol 1995;48:93–125.
[18] Vidiella B, Lázaro JT, Alsedà L, Sardanyés J. On dynamics and invariant sets in predator–prey maps. dynamical systems theory. IntechOpen; 2019.
[19] Alsedà Ll, Vidiella B, Solé R, Lázaro JT, Sardanyés J. Dynamics in a time-discrete food-chain model with strong pressure on preys. Commun Nonlin Sci Num Simul 2020;84:105187.
[20] Sardanyés J, Fontich E. On the metapopulation dynamics of autocatalysis: extinction transients related to ghosts. Int J Bifurcation Chaos 2010;120(4):1–8.
[21] Hastings A, Higgins K. Persistence of transients in spatially structured ecological models. Science 1994;263:1133–6.
[22] Crutchfield JP, Kaneko K. Are attractors relevant to turbulence? Phys Rev Lett 1988;60:2715–8.
[23] Ruxton GD, Doebeli M. Spatial self-organization and persistence of transients in a metapopulation model. Proc R Soc Lond B 1996;263:1153–8.
[24] Kuznetsov YA. Elements of applied bifurcation theory. 2nd Ed.. New York: Springer; 1998.
[25] Strogatz SH. Nonlinear dynamics and chaos with applications to physics, biology, chemistry, and engineering. Westview Press; 2000.
[26] Scheffer M, Carpenter S, Foley JA, Folke C, Walker B. Catastrophic shifts in ecosystems. Nature 2001;413:591–6.
[27] Scheffer MG, Carpenter SR. Catastrophic regime shifts in ecosystems: linking theory to observation. Ann Pol Math 2003;18:648–56.
[28] Scheffer MG, Carpenter SR. Early warning signals for critical transitions. Nature 2009;461(2009):53–9.
[29] Rietkerk M, Dekker SC, de Ruiter PC, van de Koppel J. Self-organized patchiness and catastrophic shifts in ecosystems. Science 2004;305:1926–9.
[30] Staver AC, Archibald S, Levin SA. Anticipating critical transitions. Science 2011;334:230–2.
[31] Carpenter, et al. Early warnings of regime shifts: A whole ecosystem experiment. Science 332:709–108.
[32] Trickey ST, Virgin LN. Bottlenecking phenomenon near a saddle–node remnant in a Duffing oscillator. Phys Lett A 1998;248:185–90.
[33] Valling S, Krauskopf B, Fordell T, Lindberg ÅM. Experimental bifurcation diagram of a solid state laser with optical injection. Opt Commun 271:532–42.
[34] Dai L, Vorselen D, Korolev KS, Gore J. Generic indicators of loss of resilience before a tipping point leading to population collapse. Science 2012;336:1175–7.
[35] Strogatz SH, Westervelt RM. Predicted power laws for delayed switching of charge density waves. Phys Rev B 1989;40(15):10501–8.
[36] Fontich E, Sardanyés J. General scaling law in the saddle–node bifurcation: a complex phase space study. J Phys A 2008;41(1):015102.
[37] Duarte J, Januário C, Martins N, Sardanyés J. Scaling law in saddle–node bifurcations for one-dimensional maps: a complex variable approach. Nonlinear Dynam 67:541–7.
[38] Canela J, Fagella N, Ll Alsedà, Sardanyés J. Dynamical mechanism behind ghosts unveiled in a map complexification. Chaos Solitons Fractals 2022;156:111780.
[39] Sardanyés J, Solé RV. Delayed transitions in non-linear replicator networks: About ghosts and hypercycles. Chaos Solitons Fractals 2007;31(2):307–15.
[40] Leonel ED. Defining universality classes for three different local bifurcations. Commun Nonlinear Sci Numer Simulat 2016;39:520–8.
[41] Gimeno J, Jorba A, Sardanyés J. On the effect of time lags on a saddle–node remnant in hyperbolic replicators. J Phys A 2018;51:385601.
[42] Sardanyés J, Raich C, Alarcón T. Noise-induced stabilization of saddle–node ghosts. New J Phys 2020;22:093064, 2020.
[43] Kéfi S, Rietkerk M, Alados CL, Pueyo Y, Papanastasis VP, ElAich A, et al. Spatial vegetation patterns and imminent desertification in Mediterranean arid ecosystems. Nature 2007;449(7159):213–7.
[44] Berdugo M, Delgado-Baquerizo M, Soliveres S, Hernández-Clemente R, Zhao Y, Gaitán JJ, et al. Global ecosystem thresholds driven by aridity. Science 2020;367(6479):787–90.
[45] Berdugo M, Vidiella B, Solé RV, Maestre FT. Ecological mechanisms underlying aridity thresholds in global drylands. Funct Ecol 2022;36(1):4–23.
[46] Berdugo M, Gaitán JJ, Delgado-Baquerizo M, Crowther TW, Dakos V. Prevalence and drivers of abrupt vegetation shifts in global drylands. Proc Natl Acad Sci 2022;e2123393119.
[47] Barker JL, Bronstein JL, Friesen ML, Jones EI, Reeve HK, Zink AG, et al. Synthesizing perspectives on the evolution of cooperation within and between species. Evol 2017;71–4:814–25.
[48] Allee WC. Bowen E studies in animal aggregations: mass protection against colloidal silver among goldfishes. J Exp Zool 1932;61(2):185–207.
[49] Dugatkin LA. Animal cooperation among unrelated individuals. Naturwiss 2002;89:533–41.
[50] Cassill DL, Butler J, Vinson SB, Wheeler DE. Cooperation during prey digestion between workers and larvae in the ant. Pheidole Padonia Insect Soc 2005;52:339–43.
[51] Chen MK, Hauser M. Modeling reciprocation and cooperation in primates: Evidence for a punishing strategy. J Theoret Biol 2005;235:5–12.
[52] Ruppert EE, Fox RS, Barnes RD. Invertebrate zoology. 7th ed.. Cengage Learning; 2004, p. 112–48.
[53] Ungefroren H. Autocrine TGF-β in cancer: Review of the literature and caveats in experimental analysis. Int J Mol Sci 2021;22(2):977.
[54] Solé R, Saldaña J, Montoya JM, Erwin DH. Simple model of recovery dynamics after mass extinction. J Theoret Biol 2010;267(2):193–200.
[55] Ziraldol R, Mal L. A mathematical model for apoptotic switch in Drosophila. Phys Biol 2015;12(5):056003.
[56] Groenenboom MAC, Hogeweg P. Space and the persistence of male-killing endosymbionts in insect populations. Proc R Soc Lond B 2002;269:2509–18.
[57] Kaneko K. Supertransients, spatiotemporal intermittency and stability of fully developed spatiotemporal chaos. Phys Lett A 1990;149(2–3):105–12.
[58] Sardanyés J, Solé R. Bifurcations and phase transitions in spatially-extended two-member hypercycles. J Theoret Biol 2006;243:468–82.
[59] Sardanyés J, Piñero J, Solé R. Habitat loss-induced tipping points in metapopulations with facilitation. Pop Ecol 2019;61(4):436–49.
[60] Eigen M, Schuster P. The hypercycle, a principle of natural self-organization. Springer-Verlag; 1979.
[61] Opial Z. Sur les périodes des solutions de l'équation différentielle $x + g(x) = 0$. Ann Polonici Math 1961;10(1):49–72.
[62] Chafee N. Asymptotic behavior for solutions of a one-dimensional parabolic equation with homogeneous Neumann boundary conditions. J Differential Equations 1975;18:111–34.
[63] Chow SN, Wang D. On the monotonicity of the period function of some second order equations. ČasopisProPěstovÁníMatematiky 1986;111(1):14–25.
[64] Hale JK. Asymptotic behavior of dissipative systems. In: Mathematical surveys and monographs, vol. 25, Providence, RI: American Mathematical Society; 1988.
[65] Henry D. Geometric theory of semilinear parabolic equations. In: Lecture notes in mathematics, Vol. 840. Berlin-New York: Springer-Verlag; 1981.
[66] Britton NF. Reaction–diffusion equations and their applications to biology. London: Academic Press, Inc. [Harcourt Brace Jovanovich, Publishers]; 1986.
[67] Kot M. Elements of mathematical ecology. Cambridge: Cambridge University Press; 2001.
[68] Casten RG, Holland CJ. Instability results for reaction diffusion equations with Neumann boundary conditions. J Differential Equations 1978;27(2):266–73.
[69] Matano H. Asymptotic behavior and stability of solutions of semilinear diffusion equations. Publ Res Inst Math Sci 1979;15(2):401–54.
[70] Levin SA. Dispersion and population interactions. Amer Nat 1974;108(960):207–28.
[71] Skellam JG. Random dispersal in theoretical populations. Biometrika 1951;38(1/2):196–218.
[72] Turing AM. The chemical basis of morphogenesis. Phil Trans R Soc London (B) 1952;237:37–72.
[73] Durrett R, Levin SA. The importance of being discrete (and spatial). Theor Pop Biol 1990;46(3):363–94.
[74] Kareiva P. Population dynamics in spatially complex environments: theory and data. Phil Trans R Soc Lond B 1990;330:175–90.
[75] Dieckmann U, Law R, Metz J, editors. The geometry of ecological interactions: simplifying spatial complexity (cambridge studies in adaptive dynamics). Cambridge: Cambridge University Press; 2000.
[76] Lin J, Andreasen V, Casagrandi R, Levin SA. Traveling waves in a model of influenza a drift. J Theor Biol 2003;22(4):437–45.
[77] Zhuang Q, Wang J. A spatial epidemic model with a moving boundary. Infect Dis Model 2021;6:1046–60.
[78] Boerlijst P, Hogeweg M. Spiral wave structure in pre-biotic evolution: Hypercycles stable against parasites. Physica D 1991;48:17–28.
[79] Szabó P, Scheuring I, Czárán T, Szathmáry E. In silico simulations reveal that replicators with limited dispersal evolve towards higher efficiency and fidelity. Nature 2002;420:340–3.

[80] Kim P-J, Jeong H. Spatio-temporal dynamics in the origin of genetic information. Physica D 2005;203:88–99.
[81] Sardanyés J, Solé RV. The role of cooperation and parasites in non-linear replicator delayed extinctions. Chaos Solitons Fractals 2007;31(5):1279–96.
[82] Lion S, Baalen Mv. Self-structuring in spatial evolutionary ecology. Ecol Lett 2008;11(3):277–95.
[83] Kuramoto Y. Diffusion-induced chaos in reaction systems. Progr Theoret Phys 1978;64:346–67.
[84] Pascual M. Diffusion-induced chaos in a spatial predator–prey system. Proc R Soc Lond B 1993;251:1–7.
[85] Cronhjort MB, Blomberg C. Cluster compartmentalization may provide resistance to parasites for catalytic networks. Physica D 1997;101:289–98.
[86] Sardanyés J, Solé RV. Spatio-temporal dynamics in simple asymmetric hypercycles under weak parasitic coupling. Physica D 2007;231(2):116–29.
[87] Sardanyés J. Ghosts in high dimensional non-linear dynamical systems: The example of the hypercycle. Chaos Solitons Fractals 2009;39(1):92–100.
[88] Engel KJ, Nagel R. One-parameter semigroups for linear evolution equations. In: Graduate texts in mathematics. Springer; 2000.